TU Delft

Delft University of Technology

The Modeling of the Flow Behavior Below and Above the Two-Phase Region for Two Newly Developed Meta-Stable beta Titanium Alloys

Li, Cong; Ding, Zhili; van der Zwaag, Sybrand

DOI
10.1002/adem.201901552

Publication date
2021

Document Version
Final published version

Published in
Advanced Engineering Materials

Citation (APA)
Li, C., Ding, Z., & van der Zwaag, S. (2021). The Modeling of the Flow Behavior Below and Above the Two-Phase Region for Two Newly Developed Meta-Stable beta Titanium Alloys. *Advanced Engineering Materials*, *23*(1), Article 1901552. https://doi.org/10.1002/adem.201901552

Important note
To cite this publication, please use the final published version (if applicable).
Please check the document version above.

Copyright
Other than for strictly personal use, it is not permitted to download, forward or distribute the text or part of it, without the consent of the author(s) and/or copyright holder(s), unless the work is under an open content license such as Creative Commons.

Takedown policy
Please contact us and provide details if you believe this document breaches copyrights.
We will remove access to the work immediately and investigate your claim.

This work is downloaded from Delft University of Technology.
For technical reasons the number of authors shown on this cover page is limited to a maximum of 10.

Green Open Access added to TU Delft Institutional Repository

'You share, we take care!' - Taverne project

https://www.openaccess.nl/en/you-share-we-take-care

Otherwise as indicated in the copyright section: the publisher is the copyright holder of this work and the author uses the Dutch legislation to make this work public.

ADVANCED ENGINEERING MATERIALS
www.aem-journal.com

The Modeling of the Flow Behavior Below and Above the Two-Phase Region for Two Newly Developed Meta-Stable β Titanium Alloys

Cong Li, Zhili Ding, and Sybrand van der Zwaag*

Isothermal hot compression tests of two promising new titanium alloys (Ti-10 V-1Fe-3Al and Ti-10 V-2Cr-3Al) are performed using a TA DIL805D deformation dilatometer at temperatures in and above the two-phase α + β region (730–880 °C) at strain rates ranging from 10^{-3} to 10^{-1} s^{-1}. Results show that the flow stress of the two alloys decreases with increasing deformation temperature and decreasing strain rate. Some of the flow curves manifest clear discontinuous yielding and flow softening, both of which are strongly affected by the deformation conditions. The flow stress behavior of these two alloys can be described very well by a hyperbolic–sine Arrhenius equation. When deforming in the α + β phase region, the deformation mechanism is governed by the bending or globularization of the α phase. When deforming in the pure β phase field, the flow behavior is mainly determined by dynamic recovery or recrystallization. The difference in alloy composition has a minor effect on their hot working behavior.

1. Introduction

Titanium alloys are an important structural material which has been developed and applied since the middle of the 20th century. Because of their low density, high, yet tunable specific strength, excellent corrosion resistance, good ductility at low temperatures, and good biocompatibility, they have been widely used in aerospace engineering, chemical industry, weapon industry, and biomedical fields.[1,2] The optimization of their properties by tuning the chemical composition (dictating both the β-transus and the martensite start, M_s, temperatures) and the hot deformation conditions, in particular the strain rate and the deformation temperature with respect to the β-transus temperature, has been an active research topic for several decades,[3–6] in particular for dual-phase alloys.[7,8] The deformation mechanisms and microstructural evolutions of existing commercial dual-phase titanium alloys are relatively well documented.[9] Gupta et al. have studied the evolution of microstructure and texture in Ti-15V-3Cr-3Sn-3Al alloy during cold-rolling and cross-rolling; it was found that the strain path has a strong effect on the deformation microstructure.[10] Mishra and co-workers have investigated the hot deformation behavior of a commercial grade Ti-6Al-4V with lamellar and equiaxed starting microstructures; the deformation behavior correlation of these two morphologies have been demonstrated by the Zener–Hollomon relationship.[11] Roy and Suwas have analyzed the hot deformation behavior of a hypoeutectic Ti-6Al-4V-0.1B alloy; the influence of temperature and strain rate was revealed.[12] The thermomechanical processing of welded α + β Ti-Al-Mn alloy and its effect on microstructure and mechanical properties were studied by Murthy et al.; the structural changes during welding and the various post-weld treatments and their effect on the two mechanical properties were discussed.[13] Banerjee and co-workers have investigated the high-temperature deformation processing of Ti-24Al-20Nb; power dissipation maps have been generated.[14]

Compared with other structural metals, such as aluminum alloy and steel, titanium alloys have a narrow processing "window". Normally, the microstructure of titanium alloys cannot be changed significantly by thermal deformation in the α + β phase region. Only when the deformation temperature is close to the β-transus temperature, can the microstructure be modified significantly.[15] Philippart and Rack have investigated the deformation mechanisms of Ti-6.8Mo-4.5Fe-1.5Al alloy at high temperatures and as a function of the strain rate.[16] Jia et al. have conducted isothermal compression tests on Ti60 alloy in a temperature range of 960–1100 °C and strain rate of 0.001–10 s^{-1}.[17] The high-temperature behavior and microstructural evolution of IMI834 and Ti-1100 were reported by Weisis and Semiatin.[18] Cui et al. have carried out hot compression tests for a biomedical titanium alloy Ti-6Al-7Nb.[19] All these studies revealed that the flow softening in the β phase region was weaker than that in the α + β two-phase field. This is due to the morphological changes of the α phase as well as the occurrence of dynamic recovery and

Dr. C. Li, Z. Ding
School of Energy and Power Engineering
Changsha University of Science and Technology
Changsha, Hunan 410114, China
E-mail: liconghntu@csust.edu.cn

Dr. C. Li, Prof. S. van der Zwaag
Novel Aerospace Materials Group
Faculty of Aerospace Engineering
Delft University of Technology
2629HS Delft, The Netherlands

Prof. S. van der Zwaag
Advanced Materials Institute, School of Materials Science and Engineering
Tsinghua University
Beijing 1000984, China

The ORCID identification number(s) for the author(s) of this article can be found under https://doi.org/10.1002/adem.201901552.

DOI: 10.1002/adem.201901552

 © 2020 Wiley-VCH GmbH

recrystallization.[18,19] The microstructure in the α + β phase field deformation is characteristic of refined dynamic recrystallization (DRX) α phase, whereas in the β phase field, the morphology is characteristic of refined β grains.[6] In the current study, the high-temperature deformation behavior of two novel meta-stable titanium alloys (Ti-10V-1Fe-3Al and Ti-10V-2Cr-3Al) is studied. The observed behavior is compared to that of existing dual-phase titanium alloys. These alloys were selected for their excellent and tunable mechanical behavior at room temperature when treated to the desired meta-stable state and are being considered as potential candidates for many industrial applications.[20] The purpose of the present article is to address the dynamic recovery and recrystallization behavior of the new alloys and to capture their high-temperature deformation behavior in quantitative expressions.

2. Experimental Section

The alloys (Ti-10V-1Fe-3Al and Ti-10V-2Cr-3Al) used in this work were received in the as-forged conditions and supplied by the Institute of Metal Research, Chinese Academy of Science, Shenyang, China. Each ingot weighted about 5 kg. The chemical compositions of the two alloys and their Mo_{eq} values, calculated through Equation (1),[5] are listed in **Table 1**.

$$Mo_{eq} = 1.00Mo + 0.28Nb + 0.22Ta + 0.67V + 1.6Cr + 2.9Fe - 1.00Al(wt\%) \quad (1)$$

The two alloys were solution-treated at 780, 790, 800, 810, 820 °C for 15 min, and the optical microstructures after quenching were recorded to determine the β-transus temperatures. The β-transus temperatures of theTi-10V-1Fe-3Al and Ti-10V-2Cr-3Al alloys thus determined to be ≈810 and 800 °C, respectively. The as-received slabs had been subjected to several forging passes both in the β and α + β state, resulting in homogeneous microstructures, as shown in **Figure 1**. The corresponding X-ray diffractograms are shown in Figure 1c. The morphology of in the Ti-10V-1Fe-3Al alloy is rather homogeneous and lamellar with the lamellar regions at an angle with each other. In Ti-10V-2Cr-3Al alloy, the initial microstructure shows a high volume fraction of very fine α phase, and there is some coarser lamellar α at the grain boundary. The starting microstructures resemble those reported previously for these alloys.[20,21]

Cylindrical specimens with 5 mm diameter and 10 mm length were electron discharge machined (EDM) from the ingots for compression tests. Hot compression tests using a TA DIL805D dilatometer were performed in a vacuum atmosphere over a temperature range of 730–880 °C, i.e., below and above the transus temperature at around 800 °C. Strain rates were varied between 10^{-3} and $10^{-1}\,s^{-1}$. Molybdenum discs with 8 mm diameter and 0.1 mm thickness were welded on the end surfaces of the specimens to reduce the friction between the anvil and the samples. S-type thermocouples were also welded on the middle surface of samples to measure and control the actual temperature. The specimens were heated to the target temperature with a heating rate of $10\,°C\,s^{-1}$ and homogenized for 3 min and then deformed up to 50% height reduction. To preserve the hot deformation structure, the deformed samples were quenched immediately with argon gas upon completion of the deformation cycle. An overview of all the compression experiments performed is given in **Table 2**.

Table 1. The chemical composition of the alloys studied (in wt%)[20] and the calculated Mo_{eq} values.

	V	Fe	Cr	Al	O	C	N	Ti	Mo_{eq}
Ti-10V-1Fe-3Al	9.97	0.97	–	3.02	0.11	0.051	0.014	Bal.	6.5
Ti-10V-2Cr-3Al	10.6	–	2.18	3.19	0.1	0.05	0.013	Bal.	7.4

The deformed specimens were axially cut parallel to the compression axis and embedded in a cold-setting resin and prepared according to standard metallographic preparation methods for titanium alloys. Kroll's reagent (3 mL HF + 6 mL HNO_3 + 100 mL H_2O) was used as the etchant. A Leica LF7M38 optical microscope and a high-resolution JEOL scanning electron microscope were used to determine the microstructures as a function of the deformation conditions.

3. Results and Discussion

3.1. Flow Stress Behavior

Figure 2 shows the selected hot compression stress–strain curves of both titanium alloys at various deformation temperatures (730, 760, 790, 820, 850, 880 °C) and strain rates (10^{-1}, 10^{-2}, $10^{-3}\,s^{-1}$).

For some curves, in particular those at the lower end of the temperature scale explored, the stress increases rapidly at the beginning and then starts to decrease with the continuous increase of strain until a steady-state stage is obtained. For such curves, the strengthening effect due to dislocation pile-up is greater than that of dynamic softening, resulting in work hardening, and the flow stress increases rapidly with increasing strain. Upon a further increase in the total deformation, i.e., when the dislocation density increases, softening mechanisms such as dynamic recovery and DRX play a more dominant role, which makes the flow stress begin to decrease. During the process of loading, part of deformation energy will be stored by dislocations and other defects. This part of energy will be released as the driving force of the dynamic recovery and recrystallization. Therefore, continuous increase in dislocation density also accelerates the dynamic recovery and dynamic crystallization. In this stage, work hardening and softening mechanisms interact and offset each other. Finally, a dynamic equilibrium is reached.

From Figure 2, it can also be found the high-temperature deformation curves clearly show discontinuous yielding phenomena. This behavior refers to the sudden drop of flow stress when the flow stress reaches its peak value. When the strain rate is $10^{-1}\,s^{-1}$, samples deformed at 760 °C start to present the discontinuous yielding phenomena. Yet, when the strain rate is $10^{-3}\,s^{-1}$, until 820 °C, the stress–strain curves begin to yield discontinuously. The higher the deformation temperature and strain rate, the more clear the discontinuous yield phenomenon. In general, there are two theories to explain this phenomenon:[17] The first is a static theory, which assumes that dislocations are blocked by solute atoms, and that at a certain stress level, these dislocations can be unlocked from the pinning centers, resulting in a sudden drop in flow stress. However, one could argue that it

© 2020 Wiley-VCH GmbH

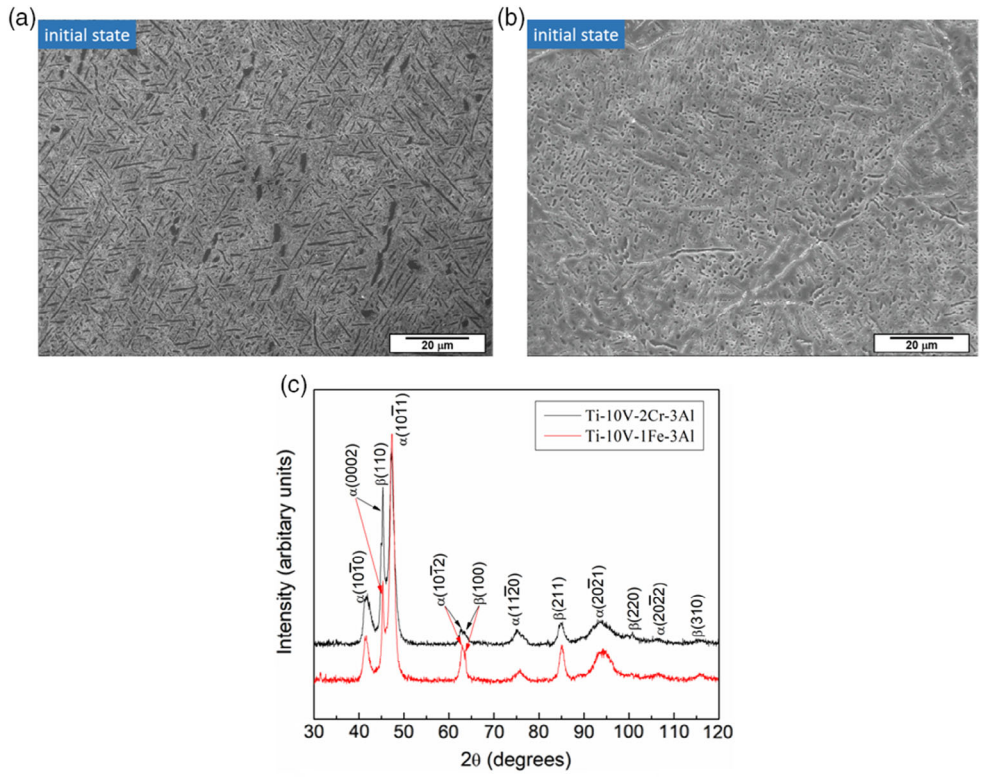

Figure 1. As-received microstructures of two the alloys a) Ti-10V-1Fe-3Al, b) Ti-10V-2Cr-3Al, c) corresponding XRD diffractograms with all peaks indexed. No unaccountable peaks were observed.

Table 2. Summary of the deformation conditions imposed.

Deformation temperature		730 °C	760 °C	790 °C	820 °C	850 °C	880 °C
Strain rate	0.1	√	√	√	√	√	√
	0.05	√	N/A	√	√	N/A	√
	0.01	√	√	√	√	√	√
	0.005	√	N/A	√	√	N/A	√
	0.001	√	√	√	√	√	√

is difficult for solid solution atoms to lock the dislocations effectively at high temperatures. Moreover, the discontinuous yield phenomena of these two titanium alloys became clearer at higher temperatures, so the static theory does not provide a reasonable explanation for the current results. The second is a dynamic theory, which is based on the assumption that discontinuous yielding is related to the rapid generation of numerous movable dislocations from grain boundaries. According to this assumption, during deformation, initially a large fraction of the dislocations is blocked by grain boundaries and accumulates there, resulting in a sharp increase in flow stress. When the dislocation density reaches a critical value, the dynamic recovery in the β phase increases rapidly, resulting in a significant decrease in flow stress and discontinuous yielding.[16] The precondition of discontinuous yielding is that the dislocation density must reach a critical level and a high strain rate is needed to ensure the dislocation accumulation, which explains the correlation between discontinuous yielding and the (high) strain rate. As shown in Figure 2, the higher the strain rate, the clearer the discontinuous yielding. The sharp decrease in movable dislocations is caused by the sudden increase in dynamic recovery. Therefore, the higher the temperature, the greater the driving force of dynamic recovery and clearer the discontinuous yielding phenomenon; this was also well reflected in every image of Figure 2. It can be concluded that the discontinuous yielding behavior of both alloys observed here can be well explained by the dynamic theory.

In addition, it was shown in Figure 2 that some of the curves have the characteristics of flow softening; that is, with the increase in strain, the flow stress decreases continuously. This phenomenon is common in high-temperature deformation of titanium alloys. Existing studies show that there are several reasons for flow softening: a change in the phase morphology, dynamic recovery and DRX, and/or a temperature rise due to adiabatic heating.[15] In general, adiabatic heating and microstructure evolution are the main causes of this behavior. The adiabatic effect usually plays a major role when strain rate is higher than $10\,s^{-1}$. When the strain rate is lower ($<10\,s^{-1}$), i.e., under the conditions of the current study, the microstructural evolution dominates. For a given deformation temperature, the flow softening effect at a high strain rate is stronger than that at a low strain rate. This can be explained as follows: at a certain deformation temperature, when the strain rate is higher, the time required for the specimen to reach a certain deformation amount is shortened and the dislocation generation rate increases. These dislocations interlace and tangle with each other, resulting in an

© 2020 Wiley-VCH GmbH

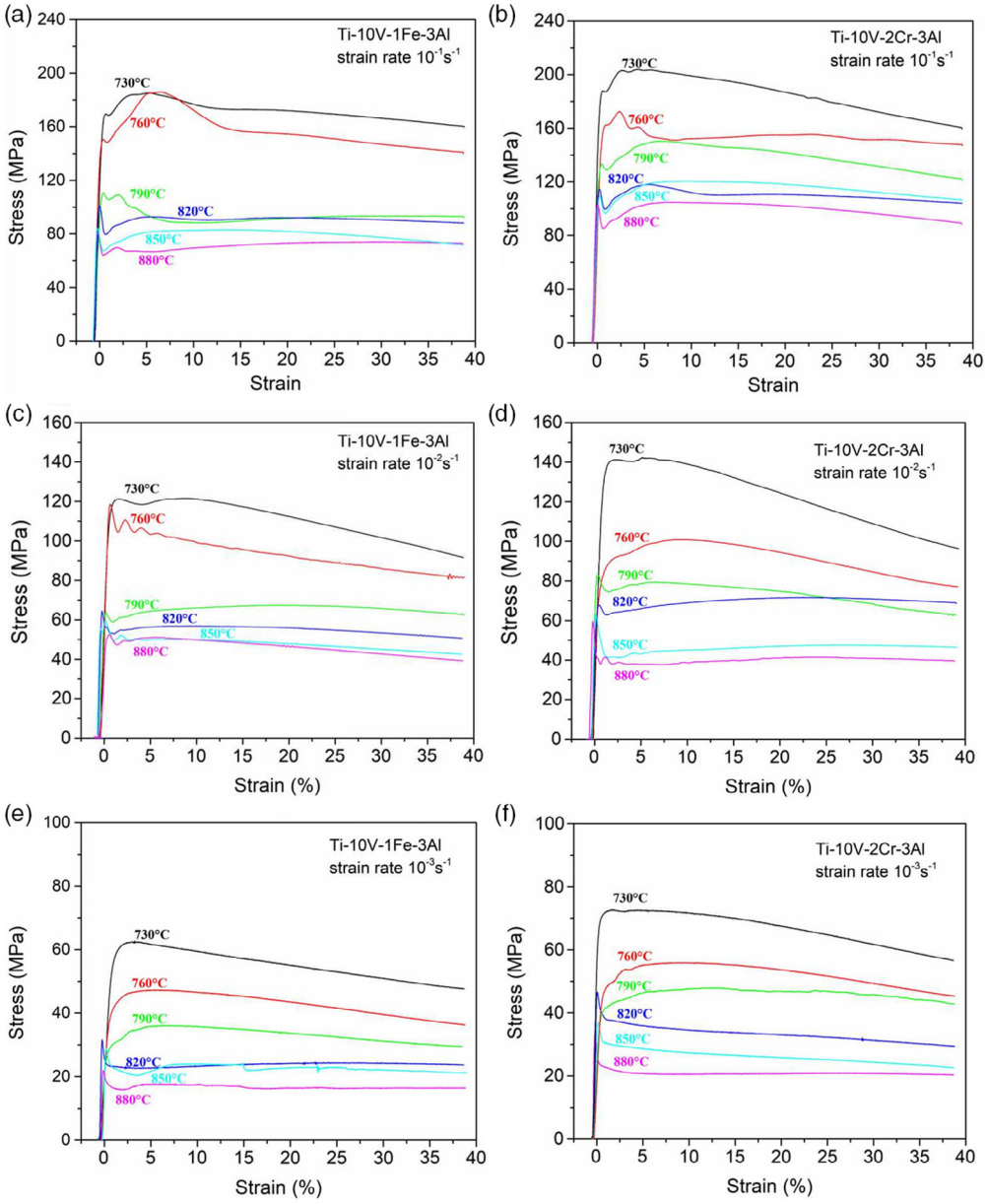

Figure 2. Selected stress–strain curves at different deformation temperatures and strain rates. a) Ti-10V-1Fe-3Al alloy deformed at the strain rate of 0.1 s^{-1}, b) Ti-10V-2Cr-3Al alloy deformed at the strain rate of 0.1 s^{-1}, c) Ti-10V-1Fe-3Al alloy deformed at the strain rate of 0.01 s^{-1}, d) Ti-10V-2Cr-3Al alloy deformed at the strain rate of 0.01 s^{-1}, e) Ti-10V-1Fe-3Al alloy deformed at the strain rate of 0.001 s^{-1}, and f) Ti-10V-2Cr-3Al alloy deformed at the strain rate of 0.001 s^{-1}.

increment in the critical stress for further plastic deformation. With a further increase in strain, various softening mechanisms gradually weaken the hardening effect until equilibrium state is reached; consequently, a stronger flow softening behavior is detectable. When the strain rate is fixed, with increasing deformation temperature, both the flow stress and the degree of flow softening decrease. Compared with the deformation in the β phase region, the flow softening is clearer in the α + β phase region. The change in the extent of flow softening with increase in temperature is the result of an ongoing microstructural evolution, which will be presented in more detail in Section 3.5.

3.2. Effect of Deformation Temperature

Figure 3 shows the effect of deformation temperature on the flow stress at three strain rates (0.1, 0.01, 0.001 s^{-1}). To show the flow stress more accurately, the stress values at the strain of 0.15, 0.25, and 0.35 are plotted in Figure 3a,b for both alloys. It can be seen that the flow stress decreases with an increase in deformation temperature, but the rate of decrement varies in different temperature ranges. In α + β phase field, the flow stress decreases rapidly, whereas in the high-temperature region (β phase field), the decrease is relatively mild. This is related to the difference in

© 2020 Wiley-VCH GmbH

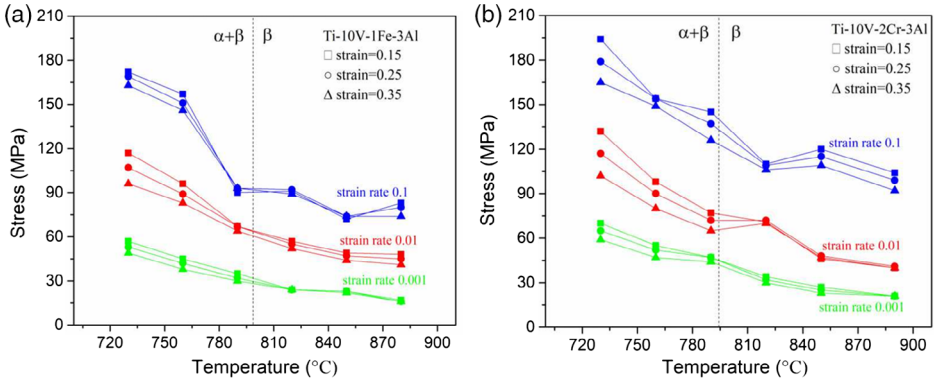

Figure 3. Effect of deformation temperature on the flow stress a) Ti-10V-1Fe-3Al, b) Ti-10V-2Cr-3Al.

microstructural stability of titanium alloys in different temperature ranges. In α + β phase field, the change in temperature will lead to a change in the volume fractions of the two phases, which will seriously affect the mechanical properties. However, in the β phase field, a change in temperature only affects the grain size of the β phase and this has a minor influence on the high-temperature flow behavior. These assumptions will be confirmed by the results of microstructure observation to be presented in Section 3.5.

3.3. Effect of Strain Rate

As shown in Figure 2, the flow stress is strongly affected by the strain rate. At a given temperature, the flow stress increases with increasing strain rate. The influence of strain rate on the flow stress can be captured by Equation (2)[22]

$$\dot{\varepsilon} = A\rho \mathbf{b}\sigma^m \tag{2}$$

where the$\sigma$is the flow stress, $\dot{\varepsilon}$ is the strain rate, ρ is the dislocation density, **b** is the Burgers vector of dislocations. But at different temperatures, the sensitivity of the flow stress to the strain rate is different. To quantitatively investigate the effect of strain rate on flow stress, a strain rate sensitivity exponent m is introduced which is defined by Equation (3)[23]

$$m = \frac{\partial \ln \sigma}{\partial \ln \dot{\varepsilon}} \tag{3}$$

The flow stress (for a fixed strain of 0.25) as a function of strain rate is plotted in a lnσ-ln$\dot{\varepsilon}$ scale, as shown in **Figure 4**. The strain rate sensitivity exponent m was calculated for each condition. It can be seen that for Ti-10V-1Fe-3Al alloy, when deformation temperature is below the β-transus (i.e., 730 and 790 °C), the m value is around 0.2 and does not change too much. When the temperature is in the β phase region, the m value increases strongly, from 0.196 at 790 °C to 0.296 at 820 °C, and finally to 0.34 at 880 °C. In Ti-10V-2Cr-3Al alloys, although the m value increases with the increase in deformation temperature, the variation is very slight when the β-transus point is crossed, from 0.267 at 790 °C to 0.276 at 820 °C. For the Ti-10V-1Fe-3Al alloy, the behavior is different and there is a marked jump at the β-transus temperature. From these analyses, it can be concluded that the flow stress of the alloy during high-temperature deformation is affected by both temperature and strain rate.

3.4. The Calculations of Constitutive Equations

To quantify the mechanical behavior of Ti-10V-2Cr-3Al alloy more quantitatively, the stress–strain curves obtained from the hot deformation under different temperature and strain rate have been fitted to constitutive equations which have been used to establish the thermo-mechanical response during hot working. The Sellars and Tegart hyperbolic–sine Arrhenius equation is used here to describe the relationship between the flow stress and various deformation parameters[24]

$$\dot{\varepsilon} = A[\sinh(\alpha\sigma)]^n \exp\left(-\frac{Q}{RT}\right) \tag{4}$$

where $\dot{\varepsilon}$ is the strain rate (s^{-1}), σ is the flow stress (MPa), R is gas constant (8.314 J mol^{-1}·K), T is the absolute temperature (K), and Q is the apparent activation energy (J mol^{-1}), A and α are materials constant. α can be calculated by Equation (5)

$$\alpha = \frac{\beta}{x} \tag{5}$$

where x and β can be calculated through Equation (6) and (7)

$$\dot{\varepsilon} = A_1\sigma^x \exp\left(-\frac{Q}{RT}\right) \tag{6}$$

$$\dot{\varepsilon} = A_2 \exp(\beta\sigma) \exp\left(-\frac{Q}{RT}\right) \tag{7}$$

Taking logarithm on both sides of Equation (6) and (7), Equations (8) and (9) were deduced.

$$\ln \dot{\varepsilon} = x \ln \sigma + \ln A_1 - \frac{Q}{RT} \tag{8}$$

$$\ln \dot{\varepsilon} = \beta\sigma + \ln A_2 - \frac{Q}{RT} \tag{9}$$

Then the values of x and β can be obtained from the slope of ln(σ) versus ln($\dot{\varepsilon}$), and σ versus ln($\dot{\varepsilon}$), as shown in Figure 4b and **5**, respectively. Actually x is the reciprocal of the strain rate sensitivity exponent m. It should be noted that in different temperature ranges, the microstructures and deformation mechanisms of the alloys are different, so x and β are calculated separately in α + β phase field (730 and 790 °C) and β phase

© 2020 Wiley-VCH GmbH

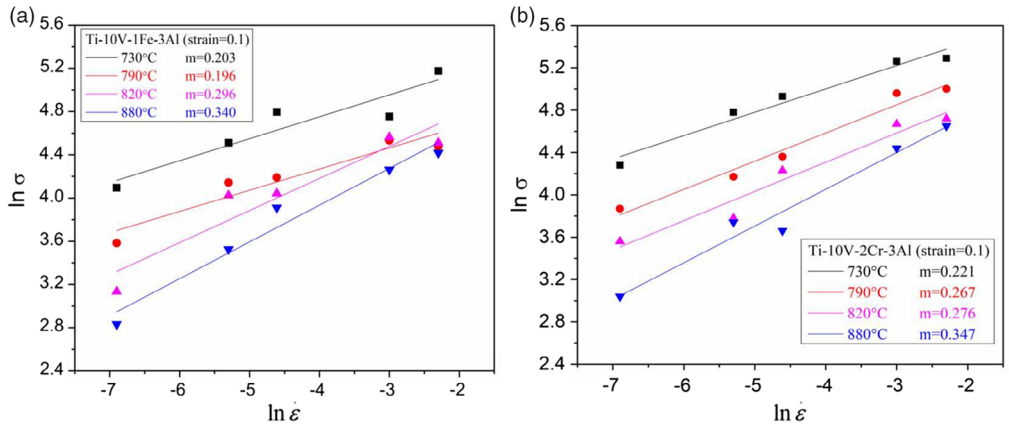

Figure 4. The strain rate exponents of a) Ti-10V-1Fe-3Al, b) Ti-10V-Cr-3Al.

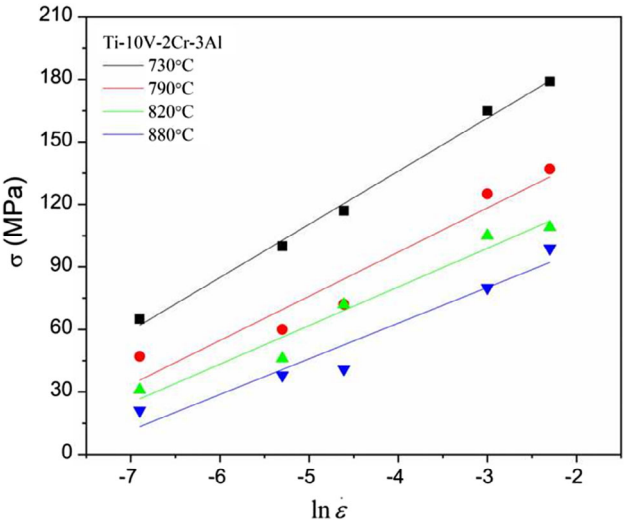

Figure 5. σ versus ln($\dot{\varepsilon}$) plot for Ti-10 V-2Cr-3Al.

Table 3. Parameter values in the constitutive equations for different alloys.

	Alloys	Phase region	n	α	lnA	Q
$\alpha+\beta$ alloys	Ti-10V-1Fe-3Al (Mo_{eq}≈6.5)	$\alpha+\beta$	3.2	0.013	37.3	366
		β	2.4	0.019	12.3	158
	Ti-10V-2Cr-3Al (Mo_{eq}≈7.4)	$\alpha+\beta$	3.2	0.014	19.8	231
		β	2.4	0.017	14.7	184
	Ti-10V-2Fe-3Al (Mo_{eq}≈8.5)[25]	$\alpha+\beta$	3.5	0.015	28.0	294
		β	2.5	0.026	13.4	185
Near α alloys	Ti-6Al-4V[28]	$\alpha+\beta$	3.5	0.009	52.6	522
		β	3.2	0.014	17.5	170
	IMI834[22]	$\alpha+\beta$	2.2	0.019	60.4	682
		β	–	–	–	–
	IMI550[29]	$\alpha+\beta$	3.4	0.023	57.9	637
		β	–	–	–	–

field (820 and 880 °C). Correspondingly, different α values are obtained for different temperature ranges. The calculation results are listed in **Table 3**.

Taking logarithmic values on both sides of Equation (4), (10) is obtained. From this the expressions of n and Q, shown in Equation (11) and (12), are obtained.

$$\ln\dot{\varepsilon} = n\ln[\sinh(\alpha\sigma)] + \ln A - \frac{Q}{RT} \tag{10}$$

$$\frac{1}{n} = \frac{\mathrm{d}\{\ln[\sinh(\alpha\sigma)]\}}{\mathrm{d}(\ln\dot{\varepsilon})} \tag{11}$$

$$Q = nR\frac{\mathrm{d}\{\ln[\sinh(\alpha\sigma)]\}}{\mathrm{d}(1/T)} \tag{12}$$

Then the values of n and Q can be obtained from the line slope of ln[sinh($\alpha\sigma$)] versus ln($\dot{\varepsilon}$), and ln[sinh($\alpha\sigma$)] versus $1/T$, respectively, as shown in **Figure 6**. The specific results are also listed in Table 3.

Using the same method, values for all parameters in the constitutive equation for Ti-10V-1Fe-3Al alloy in different temperature ranges can be determined. The apparent activation energies of Ti-10V-1Fe-3Al and Ti-10V-2Cr-3Al alloys in α + β and β phase fields are determined to be $Q_{Fe/\alpha+\beta} = 366\ \mathrm{kJ\ mol^{-1}}$, $Q_{Fe/\beta} = 158\ \mathrm{kJ\ mol^{-1}}$, $Q_{Cr/\alpha+\beta} = 231\ \mathrm{kJ\ mol^{-1}}$, $Q_{Cr/\beta} = 184\ \mathrm{kJ\ mol^{-1}}$, respectively, and these values are listed in Table 3. Theoretically, the apparent activation energy Q represents the energy barrier needed to overcome atomic diffusion. As can be seen, the activation energy in the α + β phase fields ($Q_{Fe/\alpha+\beta}$ and $Q_{Cr/\alpha+\beta}$) is higher than that of self-diffusion energy in either single α phase ($Q_{sd/\alpha} \approx 169\ \mathrm{kJ\ mol^{-1}}$) or single β phase ($Q_{sd/\beta} \approx 153\ \mathrm{kJ\ mol^{-1}}$), suggesting a complex combination of dynamic restoration processes.[15] Seshacharyulu et al. proposed that the high activation energy is related to the break-up, kinking, or globularization of lamellar structures during deformation in α + β phase field which subsequently results in flow softening.[25] Detailed observation on the deformation microstructure in Section 3.5 confirmed this deduction.

By comparing the activation energies of the two alloys, it can be found that $Q_{Fe/\alpha+\beta} > Q_{Cr/\alpha+\beta}$, which may be related to the

© 2020 Wiley-VCH GmbH

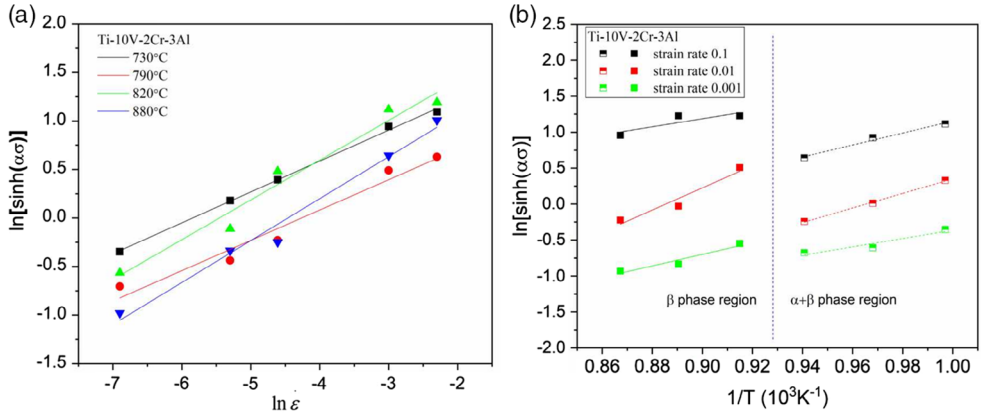

Figure 6. a) ln[sinh($\alpha\sigma$)] versus ln($\dot{\varepsilon}$) plot for Ti-10 V-2Cr-3Al, b) ln[sinh($\alpha\sigma$)] versus 1/T plot for Ti-10V-2Cr-3Al.

difference in strengthening effect of primary α phase and that of the complex interaction between alloying elements in these two alloys. On the other hand, $Q_{Cr/\beta} > Q_{Fe/\beta} \approx Q_{sd/\beta}$. It is generally assumed that when the calculated activation energy Q is close to the self-diffusion activation energy Q_{self} of pure titanium, the softening mechanism in this phase field is mainly dynamic recovery, indicating that the superplastic deformation process of large grains in the β region is controlled by diffusion. If the calculated activation energy Q is higher than Q_{self}, the softening mechanism contains DRX.[19] This preliminary conclusion is confirmed in the microstructural analysis. On the other hand, according to the research of Moneni,[26] the activation energy for hot deformation can be separated into thermal and mechanical parts. The thermal activation was found necessary to propel diffusion and help dislocations bypass the short-range barriers such as the solute atoms. The mechanical energy could help dislocations overcome strong long-range obstacles such as dislocation tangles. Here, $Q_{Fe/\beta} \approx Q_{sd/\beta}$, it implies that the $Q_{Fe/\beta}$ calculated here is almost purely thermal activation. At the same time, $Q_{Cr/\beta}$ is greater than $Q_{Fe/\beta}$, that means the Cr atoms have stronger strengthening effect than Fe atoms. With the decrease in the deformation temperature, the $Q_{\alpha+\beta}$ is found to be higher than the corresponding Q_{β}; it can be concluded that $Q_{\alpha+\beta}$ has apparently two parts, thermal and mechanical parts. It is consistent with the conclusions of the reference.

After reformulation, Equation (4) can be converted into Equation (13), the left-hand side of which is the Zener–Holloman parameter. It is an important parameter to characterize the effect of temperature and strain rate on the deformation behavior of materials. Taking logarithms on both sides of Equation (13), (14) can be obtained.

$$\dot{\varepsilon} \exp\left(\frac{Q}{RT}\right) = A[\sinh(\alpha\sigma)]^n \tag{13}$$

$$\ln Z = \ln A + n \ln[\sinh(\alpha\sigma)] \tag{14}$$

where Z is the Zener–Holloman parameter, R is the gas constant (8.314 J mol^{-1}·K). **Figure 7**a shows the relationship between ln$Z$ and ln[sinh ($\alpha\sigma$)] for two alloys. After linear fitting, the intercepts of different straight lines can be calculated to obtain the values of ln$A$ in different temperature ranges. The constitutive equations of the two alloys in different temperature region can be obtained by taking the calculated values into the Equation (4). To further verify the accuracy of the constitutive model, the experimental and calculated data of flow stress are compared, as shown in Figure 7b. A good correlation between the calculated values and the experimental values over the entire range of testing conditions is obtained.

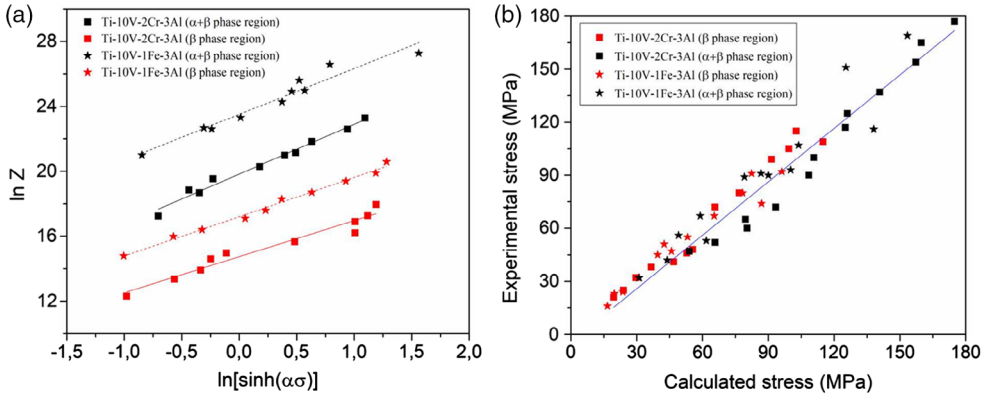

Figure 7. a) ln[sinh($\alpha\sigma$)] versus lnZ plot for two alloys, b) relationship between the calculated and experimental stress.

© 2020 Wiley-VCH GmbH

The parameter values of constitutive models applicable to conventional titanium alloys of comparable chemical composition are also listed in Table 3. Because of the high similarity in composition with the two alloys studied in this article, the reported parameter values for the Ti-10V-2Fe-3Al alloy are very close to the results calculated by us. We find that the ln$A$ and Q values of the near α alloys in α + β phase region are much higher than that of α + β alloys, while the parameters of all

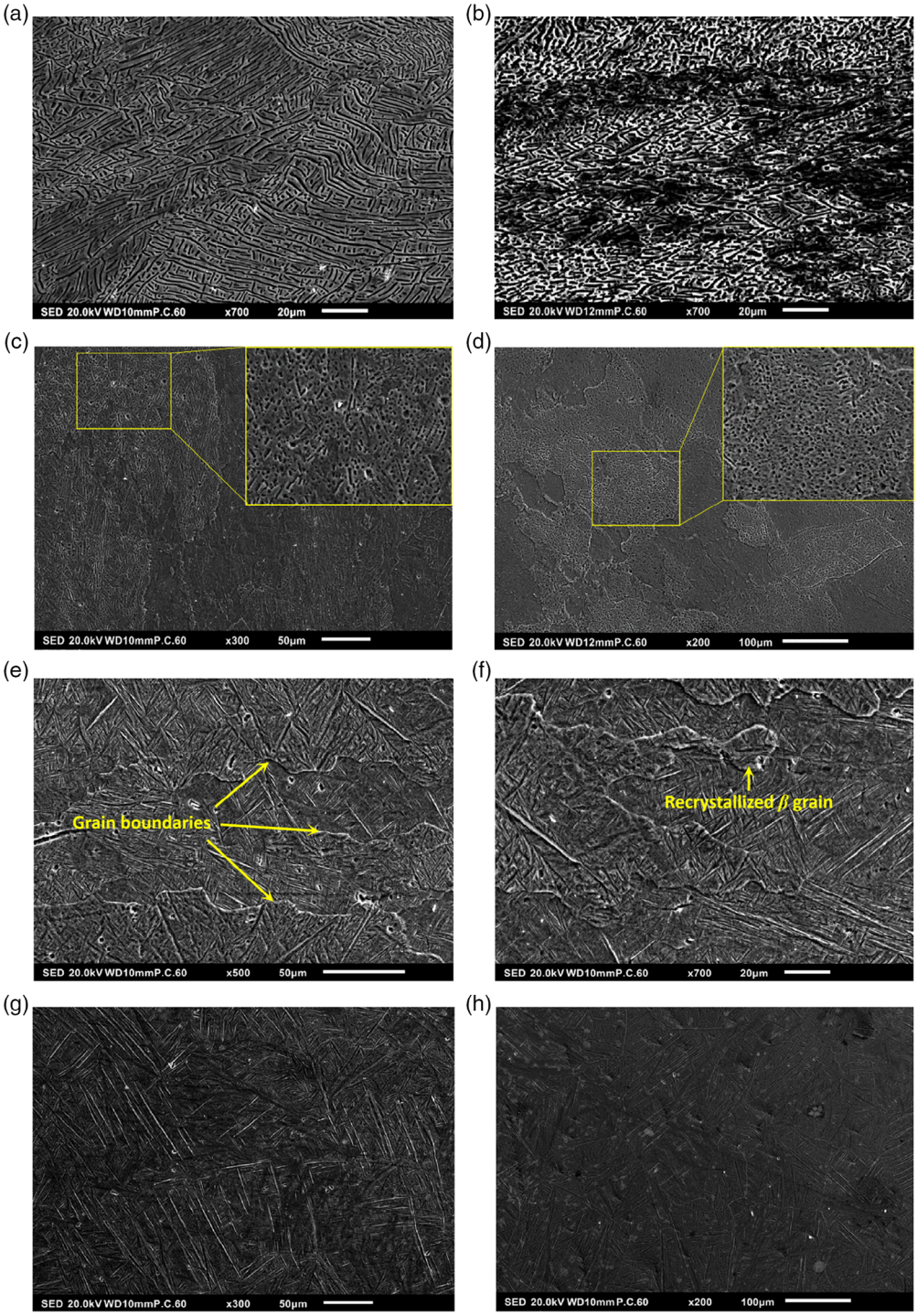

Figure 8. Deformation microstructure of two alloys: a) Ti-10V-1Fe-3Al alloy deformed at 730 °C, b) Ti-10 V-2Cr-3Al alloy deformed at 730 °C, c) Ti-10V-1Fe-3Al alloy deformed at 790 °C, d) Ti-10V-2Cr-3Al alloy deformed at 790 °C, e) Ti-10V-1Fe-3Al alloy deformed at 850 °C, f) Ti-10V-2Cr-3Al alloy deformed at 850 °C, g) microstructure of Ti-10V-1Fe-3Al alloy at 850 °C without deformation, h) microstructure Ti-10V-2Cr-3Al alloy deformed at 850 °C without deformation.

© 2020 Wiley-VCH GmbH

alloys in high-temperature β phase region are distributed over a similar range. This indicates that in the low-temperature region, the mechanical parameters of titanium alloys are strongly influenced by alloying elements and the secondary phase, including phase morphology, fraction, distribution and so on, whereas in the high-temperature β phase region, the mechanical parameters change only a little because of the invariant bcc structure of the alloys.

3.5. Observation of the Deformation Microstructures

Figure 8 shows the microstructures of the two titanium alloys deformed at different temperatures at a strain rate of $0.01\,s^{-1}$. It was found that the deformation modes of these two alloys are similar when deformed at a relatively low temperature (730 °C), as shown in Figure 8a,b. The original flat lamellar α phase was bent under compression loading, resulting in a decrease in flow stress and subsequently softening behavior. On the other hand, the dispersed α phase plays an important role in the strengthening mechanism, but in the high-temperature β phase field such effect is absent. This is why the influence of temperature on flow stress varies in different phase fields, as shown in Figure 3. Similarly, in multiphase Ti alloys such as eutectic alloys, such as Ti-Sn and Ti-Cr-Si alloys, it was found that introducing a nano-scale layer-structured matrix in the β-Ti alloys is very effective to enhance the yield strength.[1,27] With an increase in deformation temperature (790 °C), the microstructure changes dramatically. Although the deformation temperature is still in the α + β phase field, it is very close to the β-transus temperature. Under these conditions, the α phase is thermodynamically unstable and the mobility of atoms is enhanced. Therefore, α→β phase transformation and globularization of α phase occurs in both alloys, as shown in Figure 8c,d. The strain rate also has some influence on the globularization process. At a low strain rate, the deformation time is prolonged and the α→β transformation is more complete, i.e., the lamellar α phase has enough time for interface migration, and the globularization process is more fully carried out. When the temperature is increased to 850 °C, the α phase dissolves completely and dislocation slip and climb in a purely bcc phase structure becomes dominant, as shown in Figure 8e,f. Compared with the undeformed microstructure (Figure 8g,h), such as big grains, straight grain boundaries and martensite, with increasing deformation strain, the β grains become more elongated during the compression process, and dislocation piling-up occurs at the grain boundary. The later results in a local stress concentration at the grain boundary, as a result of which, the original straight grain boundaries are destroyed and become serrated. It is observed that the dynamic recovery is the main softening process in Ti-10V-1Fe-3Al alloy, while some fine recrystallized grains can be found in Ti-10V-2Cr-3Al alloy. This phenomenon is consistent with the previous inference from the apparent activation energy. In general, it can be concluded that the high-temperature deformation mechanism of these two alloys is greatly affected by the compression temperature. However, within the somewhat limited scope of this study, the strain rate itself has a minor effect on the deformation mechanism. Both phenomena are comparable to those encountered in other dual-phase titanium alloys.

4. Conclusion

Hot compression behavior of two newly developed meta-stable titanium alloys (Ti-10V-1Fe-3Al and Ti-10V-2Cr-3Al) both with a lamellar α starting microstructure is investigated by isothermal deformation tests in the temperature range of 730–880 °C (i.e., below and above the β-transus temperature for strain rates ranging from 0.1. to $-0.001\,s^{-1}$. The following conclusions can be drawn: 1) The flow stress of the alloys is highly affected by both temperature and strain rate. At higher deformation temperatures and strain rates, discontinuous yielding was observed, and it can be well explained by the dynamic theory. 2) The temperature-dependent softening in the α + β phase region is stronger than that in the β phase field due to the concurrent phase transformation of the α phase fraction. For a given deformation temperature, the flow softening effect at a high strain rate is stronger than that at a low strain rate. 3) The activation energy of the two alloys in the α + β phase fields is higher than that of self-diffusion energy in either single α phase or single β phase, suggesting a complex combination of dynamic restoration processes, which may be related to the difference in strengthening effect of primary α phase and that of the complex interaction between alloying elements in these two alloys. 4) In the β phase field, the dynamic recovery is the main softening process in Ti-10 V-1Fe-3Al alloy, while some fine recrystallized grains can be found in Ti-10V-2Cr-3Al alloy, and it was confirmed theoretically by the calculated activation energy.

Acknowledgements

The authors gratefully acknowledge the financial support provided by National Natural Science Foundation of China (Grant No. 51775055, 51975061), Natural Science Foundation of Hunan Province (Grant No. 2018JJ3539, 2019JJ40300), Research Foundation of Education Bureau of Hunan Province (Grant No. 19B033), China Scholarship Council (CSC), and Hunan Province 2011 Collaborative Innovation Center of Clean Energy and Smart Grid.

Conflict of Interest

The authors declare no conflict of interest.

Keywords

constitutive equations, hot compression, microstructural evolutions, titanium alloys, zener holloman parameters

Received: December 19, 2019
Revised: August 14, 2020
Published online:

[1] Y. J. Hwang, S. H. Hong, Y. S. Kim, H. J. Park, Y. B. Jeong, J. T. Kim, K. B. Kim, *J. Alloy Compd.* **2018**, *737*, 53.
[2] C. Li, M. Li, H. Li, J. Chen, H. Xiao, *Kovove. Mater.* **2020**, *58*, 41.
[3] C. Li, L. Qin, M. Li, H. Xiao, Q. Wang, J. Chen, *J. Alloy Compd.* **2020**, *815*, 152426,
[4] S. H. Hong, Y. J. Hwang, S. W. Park, C. H. Park, J. T. Yeom, J. M. Park, K. B. Kim, *J. Alloy Compd.* **2019**, *793*, 271.

© 2020 Wiley-VCH GmbH

[5] C. Li, X. Wu, J. H. Chen, S. van der Zwaag, *Mater. Sci. Eng. A* **2011**, *528*, 5854.
[6] Z. Wang, X. Wang, Z. Zhou, *J. Alloy Compd.* **2017**, *629*, 149.
[7] B. Liu, H. Matsumoto, Y. P. Li, Y. Koizumi, Y. Liu, A. Chiba, *Mater. Trans.* **2012**, *53*, 1007.
[8] A. D. Manshadi, R. J. Dippenaar, *Mater. Sci. Eng. A* **2012**, *552*, 451.
[9] K. Wang, W. Zeng, Y. Zhao, Y. Lai, Y. Zhou, *Mater. Sci. Eng. A* **2010**, *527*, 2559.
[10] A. Gupta, R. K. Khatirkar, A. Kumar, K. Thool, N. Bibhanshu, S. Suwas, *Mater. Character.* **2019**, *156*, 109884.
[11] J. S. Jha, S. P. Toppo, R. Singh, A. Tewari, S. K. Mishra, *J. Mater. Process. Tech.* **2019**, *270*, 216.
[12] S. Roy, S. Suwas, *J. Alloys Compd.* **2013**, *548*, 110.
[13] K. K. Murthy, N. C. Sekhar, S. Sundaresan, *Mater. Sci. Tech.* **1997**, *13*, 343.
[14] P. K. Sagar, D. Banerjee, K. Muraleedharan, Y. V. R. K. Prasad, *Metall. Mater. Trans. A* **1996**, *27A*, 2593.
[15] K. X. Wang, W. D. Zeng, Y. Q. Zhao, Y. J. Lai, X. M. Zhang, Y. G. Zhou, *Mater. Sci. Tech.* **2011**, *27*, 21.
[16] I. Philippart, H. J. Rack, *Mater. Sci. Eng.* **1998**, *243*, 196.
[17] W. Jia, W. Zeng, Y. Zhou, J. Liu, Q. Wang, *Mater. Sci. Eng. A* **2011**, *528*, 4068.
[18] I. Weisis, S. L. Semiatin, *Mater. Sci. Eng. A* **1999**, *263*, 243.
[19] W. F. Cui, Z. Jin, A. H. Guo, L. Zhou, *Mater. Sci. Eng. A* **2009**, *499*, 252.
[20] C. Li, H. Li, S. van der Zwaag, *Wear* **2019**, *203094*, 440.
[21] C. Li, J. H. Chen, X. Wu, W. Wang, S. van der Zwaag, *J. Mater. Sci.* **2012**, *47*, 4093.
[22] Y. Y. Zong, D. B. Shan, M. Xu, Y. Lv, *J. Mater. Process. Tech.* **2009**, *209*, 1988.
[23] I. Balasundar, T. Raghu, B. P. Kashyap, *Prog. Nat. Sci: Mater. Int.* **2013**, *23*, 598.
[24] H. J. McQueen, N. D. Ryan, *Mater. Sci. Eng. A* **2002**, *322*, 43.
[25] T. Seshacharyulu, S. C. Medeiros, W. G. Frazier, Y. V. R. K. Prasad, *Mater. Sci. Eng. A* **2002**, *325*, 112.
[26] A. Moneni, *J. Mater. Res.* **2016**, *31*, 1077.
[27] Y. S. Kim, H. J. Park, J. T. Kim, S. H. Hong, G. H. Park, J. M. Park, J. Y. Suh, K. B. Kim, *Met. Mater. Int.* **2017**, *23*, 20.
[28] D. G. Robertson, H. B. McShane, *Mater. Sci. Eng. A* **1998**, *14*, 339.
[29] J. Norley, *Ph.D. Thesis*, University of London, **1985**.

© 2020 Wiley-VCH GmbH